SSIM 2021 - PM Dight (ed.)

doi:10.36487/ACG_repo/2135_19

Geotechnical parameters for pit slopes in weak volcanic rocks on Simberi Island, Papua New Guinea

NRP Baczynski *Prime Geotechnics Pty Ltd, Australia*

JN Moncrieff *FXJ Mining Technical Services, Australia*

KA Woodward *Simberi Gold Company Limited, Papua New Guinea*

Abstract

Simberi gold mining operations occur on a 6 × 6 km island at the easternmost edge of Papua New Guinea. Rainfall is 3–5 m per year. Groundwater is variable; perched watertables establish after major rainfall events and artesian pressures exist locally. Earthquake magnitudes of 5–6 (Richter scale) occur at nearby tectonic plate boundaries; mine specific seismic risks were assessed. Lithology and structure are complex and spatially variable; rock mass is hydrothermally altered, deeply weathered and intensely brecciated. Intact rock unconfined compressive strength (UCS) is often between 1–10 MPa and variable. High strength porphyritic rocks are locally 50–140 MPa but low strength rocks often persist with depth. Simberi is traversed by numerous closely spaced sets of faults related to volcanic intrusions and plate tectonics. Initial geotechnical drilling was done in the mid-1980s and gold mining started in early 2000s. Current open pits are 120–150 m deep and extract oxide ore. Future pits will be 250–300 m deep (i.e. to 50 m below sea level) and will mine sulphide ore. Due to the shallow depth and good stability of the early pit slopes, pre-2016 external geotechnical auditing was completed on an as-required basis. However, from 2016, regular annual reviews were undertaken. The geotechnical model for the sulphide pits is based on slope mapping, orientated core drilling and laboratory testing. Major investigations were completed in 2020; a challenging task due to COVID-19 travel restrictions. Wide scatter exists in the data but UCS and rock quality designation averaged over 25 m relative level depth intervals improve linearly with depth. In general, occurrence of clayey-breccia zones abates with depth. Hoek–Brown and Step-Path rock mass strength models were considered. Investigation results, data trends, assessed parameters and pit slope models are presented and discussed.

Keywords: *RQD, UCS, weathered hydrothermally altered rocks, low strength, 300 m deep pits, Hoek–Brown, Step-Path*

1 Introduction

Simberi Island is located at the easternmost edge of Papua New Guinea (PNG). Figure 1 shows its location.

Figure 1 Locality map: Simberi Island, Papua New Guinea

The mining of oxide ore commenced on Simberi Island in the early 2000s, while future mining will extract sulphide ore. Current pit depths are 120–150 m and future pits will be 250–300 m deep, with the floors of some pits designed to be below sea level. Figure 2 shows the locations of the open pits; listed from north to south they are Sorowar, Pigiput, Pigibo, Botlu, Pigicow, Samat and Bekou, named after local geographic features.

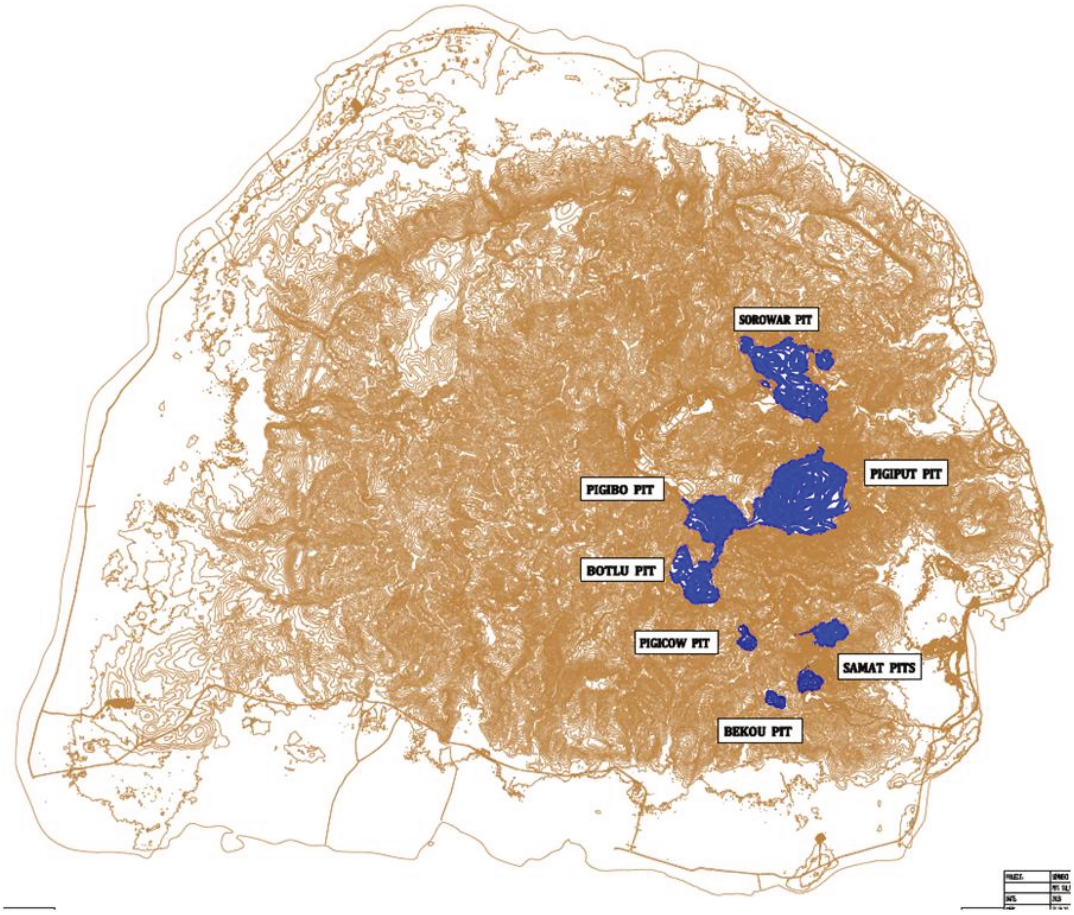

Figure 2 Open pit locations (Simberi Island approximately 6 km diameter)

Considerable geotechnical data now exists for the Simberi project. Pre-2016 investigations included Golder Associates (1996, 2003, 2010, 2011), Douglas Partners (2005), Norman (2012) and Jones (2013, 2014). Initial core logging was completed by McMahon Associates (1986) and Dames & Moore (1989) for Kennecott Niugini Mining Joint Venture, with their handwritten core logs reproduced in Golder Associates (1996, 2003).

Baczynski (2016a, 2016b, 2017 and 2018) focused on quantifying the structural geology, intact rock and rock mass strength, groundwater and seismic risks. The investigation challenge was to assess lateral and depth variability within the Simberi project area and, ideally, to simplify models to facilitate stability analyses and pit slope design.

Baczynski (2020) considered the geotechnical models for the first four listed pits; Swaisgood (2020) assessed the seismic risks. Pigiput Pit (Figure 3) is specifically discussed; with similar geotechnical models applying to the Pigibo and Botlu pits. Based on the data available at the time of writing, the Sorowar pit does not follow these geotechnical trends due, in part, to the presence of a major structure in the southern portion of the pit.

Investigation methodology, challenges and results, data trends, assessed parameters and pit slope models are presented and discussed.

Figure 3 Pigiput Pit (March 2020)

2 Methodology

During the initial 2016 geotechnical review, previous geotechnical data exhibited the following trends.

There was wide lateral and vertical scatter of rock quality designation (RQD) index, and in core logging estimated unconfined compressive strength (UCS) across the project area.

It was unlikely that geotechnical core logging completed by non-geotechnical personnel was checked. In particular, while standard UCS strength logging classes were used, medium and high strength classes have wide lower-upper ranges. UCS strength estimates could not be more narrowly refined. Relogging of old cores had limited usefulness as cores had weathered and were disturbed by splitting for assay purposes. The sighted old core was often a mixture of cobbles, gravel and fines.

Only limited laboratory UCS data existed, i.e. for the upper 25% of the sulphide pit slope profiles (Douglas Partners 2005).

No dip direction/dip angle labels were shown on the Simberi fault map; attempts to reconcile compass readings in a digital database with specific structures on the map were unsuccessful.

The observed length of structures in the database was not stated.

The 2013–2014 structural map is based on mapping in shallow (<30 m deep) open pit workings. Mapped structures were projected down 250–300 m along their dip to a relative level (RL) 0 m plane, and because structural variability exists, it was uncertain if structural patterns actually persisted with the projected depth.

The above concerns guided future work, with only some uncertainties partially resolved in 2016–2018. Initial efforts were aimed at building simple geotechnical models by rock type and by depth below the topographic ground surface but the achieved outcomes were still complex.

In an attempt to simplify models, rock mass properties were then processed with respect to same RL depth (i.e. with sea level at RL 0 m). Figure 4 shows the RL depth concept, where two boreholes BH-1 and BH-2 are collared at RL 120 m and RL 290 m with respect to sea level and one rock type exists. If geotechnical properties varied with downhole depth below borehole collar/ground surface, then RQD at depth A in Figure 4 (about 20 m below ground surface or RL 100 m) in borehole BH-1 should be similar to RQD at 20 m downhole depth (or RL 260 m) in BH-2. Conversely, if strength was related to RL depth, then UCS at depth A in BH-1 would be similar to UCS at depth B in BH-2. Likewise, geotechnical properties at depths C and D would be similar. Such RL similarity might exist if, for example, the rocks were horizontally stratified in the first

instance, but such layering was initially considered unlikely in the highly variable intrusive volcanic breccia rocks.

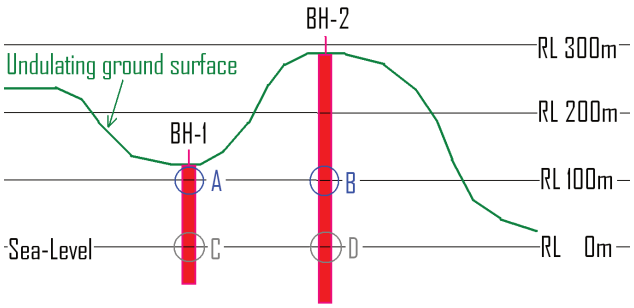

Figure 4 Borehole (BH) depth below collar versus relative level (RL) depth

Figure 5a for pre-2016 holes suggest a wave-like cyclicity in RQD trend (i.e. with wavelength ±150–200 m RL depth and amplitude RQD ±50%). Such cyclicity might reflect a situation where strata had been displaced by faults; thereby the same strata are then encountered several times in holes and/or episodic volcanic eruptions producing layered deposits of similar geotechnical morphology.

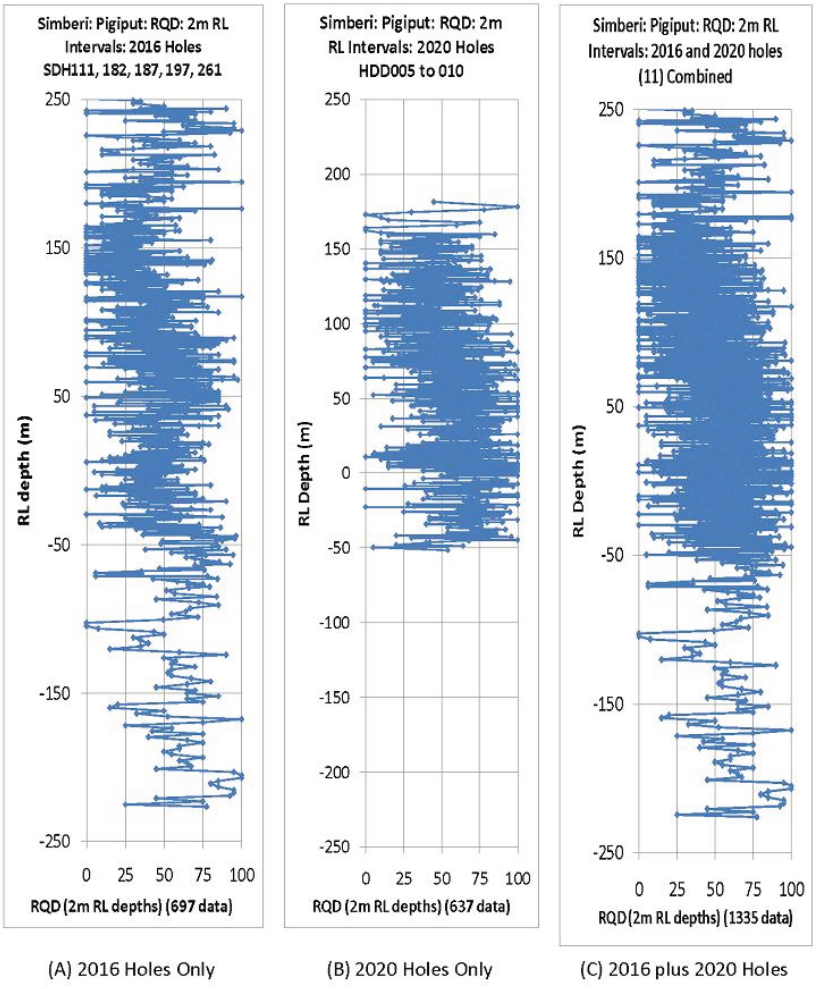

Figure 5 Pigiput Pit rock quality designation (RQD): (a) Pre-2016 holes; (b) 2020 holes only; (c) Pre-2016 and 2020 holes

The stability of the existing oxide pit slopes is very good, with the authors only aware of minor shallow slips. Most were not wedge failures but likely due to initial rainfall water runoff erosion along faults to create slope

voids/chasms and subsequent progressive attrition of ground between these voids. With this type of process, a simplistic back-analysis of the resulting wedge-shaped failure voids has little geotechnical merit.

Figure 6 is a plot of height versus overall face angle of 2016–2018 excavated slopes. These were back-analysed to assess lower-bound shear strength for weathered volcanic breccia, porphyry intrusive and mudstone.

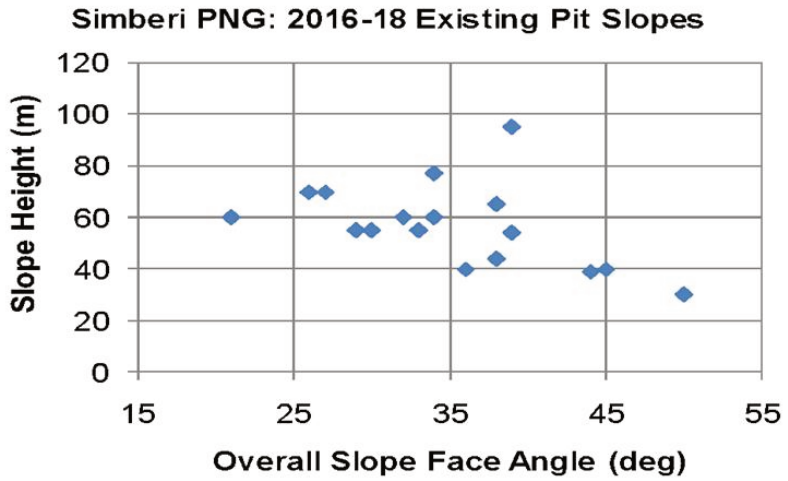

Figure 6 Simberi: as-excavated pit slopes – weathered volcanic breccia and porphyry intrusive rocks

The following investigations were pursued in 2020.

Seven cored geotechnical holes (cumulative total 1,593 m) were drilled. Six drill holes in Pigiput Pit were structurally orientated with the Reflex ACT RD II device (i.e. HDD006-HDD010 in Figure 7). Several other pre-2016 Simberi drill holes in Pigiput Pit were reviewed. One orientated core hole was in Sorowar pit.

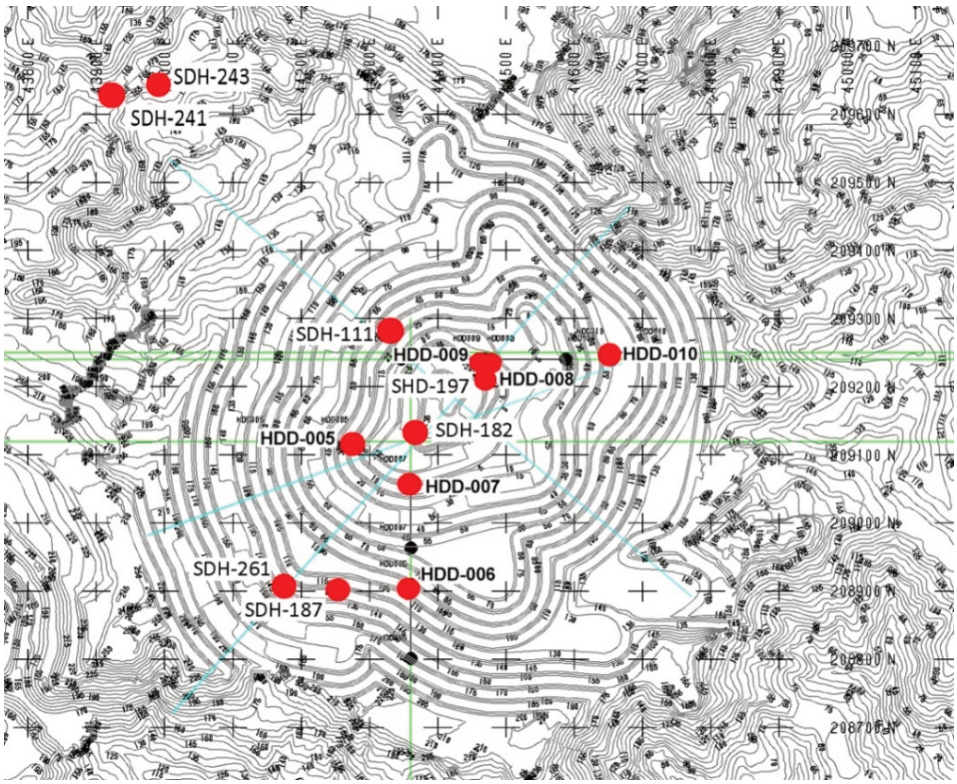

Figure 7 Pigiput sulphide pit: location of considered geotechnical drill holes (red dots)

A total of 1,230 structures were measured. Terzaghi (1965) correction factor (TCF) was applied to core data to reduce drilling direction bias on stereographic projection plots. Core data was partitioned by RL depth (i.e. ≥50 m RL and <50 m RL) to check if structural pattern varied with depth. The Exploration Geology department also orientated segments in 32 of their 2016–2019 holes with 510 structures measured. The TCF adjustment was also applied to this data.

Basic geotechnical logging (i.e. rock type, weathering, UCS, core recovery, percentage occurrence of brecciated weak zones, RQD, fractures per metre, defect angle with core axis, infill type and Barton's joint roughness) were recorded for successive 2 m core depth intervals, and representative intact rock core samples selected for offsite laboratory testing in Brisbane. Orientated core logging included hole depth, rock type, estimated rock weathering and UCS, structure type, dip direction/dip angle relative to reference line, infill type and its thickness and Barton's surface roughness; the latter as per Barton & Choubey (1977).

During the 2020 site visit, the first author photographed existing slopes and undertook slope face mapping. Photo structures were grouped by trace trends to assess lengths, large-scale surface roughness undulations, occurrence/length of rock bridges and length/width of coaligned defect zones. Slope face structural mapping by the Exploration Geology department during 2016–2019 was processed and interpreted. The latter added 500 more readings to the database. Detailed discussions were held with the Exploration Geology team who were in the process of developing a three-dimensional digital fault model for the Simberi pit workings.

Pre-2020, only a handful of cores (above RL 200 m) had been laboratory tested (Douglas Partners 2005). During 2020, more than 250 rock core samples were airfreighted to a Brisbane geotechnical laboratory; 145 of these were tested. Rock tests undertaken were UCS, Brazilian and Is(50) point-load strength and density (dry/wet). Every effort (but often unsuccessful) was made to extract undisturbed core of brecciated (soil-strength) materials for triaxial and direct shear testing (45 tests done). Ideally, weak samples should have been sampled at the drill rig, but limited site staff resources did not allow 24/7 drilling supervision. Core trays were placed in plastic bags to impede drying and were delivered to the core shed daily; promptly unwrapped, photographed, basic geotechnical/exploration logged, geotechnically sampled and structurally orientated core logged. Extracted cores were wrapped and packed to minimise disturbance/drying, with the time interval between drilling and core sample packing being 1–3 days. Ultimately, only undisturbed samples were tested; hence laboratory sample rejection rate was high for the weakest core samples.

The data was entered into an Excel spreadsheet and statistically processed to develop geotechnical models.

The initial intent was to develop Hoek–Brown and Step-Path rock mass strength models; the latter detailed in Baczynski (2019). Ultimately, only the Hoek–Brown model was adopted with the stability impact of major faults being individually considered in respective slopes. Step-Path models are difficult to develop for intact rock UCS <10 MPa because Barton's joint strength is often computed as being greater than the Hoek–Brown rock mass strength.

The earthquake risk model is based on the Swaisgood (2020) report. Slope stability was assessed via two-dimensional limiting-equilibrium GALENA 7 software.

3 Geology

The geology and fault map in Figure 8 is from Jones (2014). Updated geology plans were also generated by Simberi Exploration Geology for the open pits. A diversity of volcanic breccia types and porphyry inclusive rocks dominate in-pit slopes. Rafts and larger patches of sedimentary rocks occur locally but these comprise less than 5–10% of slope faces.

Figure 9 shows the typical appearance of the Simberi volcanic breccias.

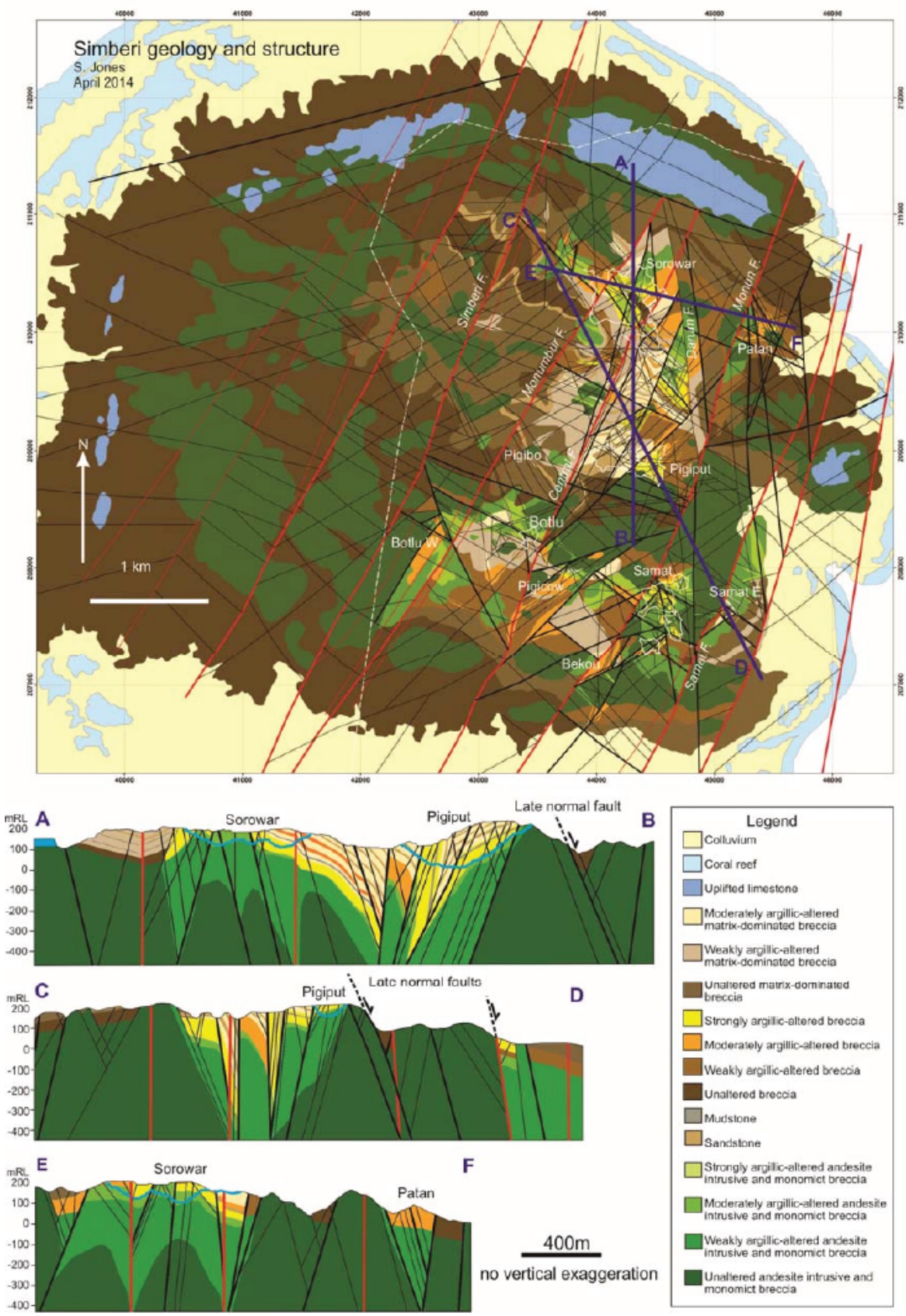

Figure 8 Simberi Island geology and major structures; per Jones (2014)

Figure 9 Sorowar Pit: volcanic breccia (camera lens cap 60 mm diameter)

4 Major and minor structures

Fieldwork since 2014 suggests that the fault pattern is far more complex than in Figure 8; with many short-range faults exposed by mining. The authors interpret that the structural patterns are due to two processes. The first is associated with volcanic intrusions (i.e. radial and tangential faults around the intrusive plugs/domes); the second is due to tectonics at nearby plate boundaries as per Jones (2013, 2014). A dual model helps to better explain the observed structural variability within the project area.

In addition to the normal faults (dipping at 55–85°) in Figure 8, slope mapping and drilling confirm that two sets of thrust faults exist. Each set comprises conjugate pairs of defects dipping in opposite directions at 20 to 35°. These structures are usually short (<5–10 m), but a 300 m+ thrust fault was mapped by site geologists.

Whilst faults, shears, contacts, bedding, other layering, joints and veins are distinguished in field mapping and core logging; the Simberi database is dominated (90–95%) by faults/shears. Stereographic projection plot patterns for minor structures mapped in pit slopes are similar to major structures but the latter exhibit flatter dips. Drag folding of strata is seen in the proximity of some major faults.

Figures 10a to 10d comprise stereographic projection plots for all pit-mapped structures combined; Figures 11a to 11d show core data. The core pattern is significantly biased by hole-drilling directions relative to structure orientations, and this bias persisted even after the TCF (Terzaghi 1965) was applied. Many steep sets in slope mapping data are only weakly represented in core data plots, but cores strongly reinforce the existence of the thrust fault sets shown in Figure 10d and confirm that the general structural pattern remains the same with increasing pit depth (compare Figures 11c and 11d).

The maximum density contour defining the mean structure orientation on stereographic projections is low (<5%), and there is a widespread of orientations around the mean. Most mapped (not core) structures have steep dip angles (i.e. >60°), while orientated core data in Figure 11 reinforces the existence of three to four sets of shallow dipping (i.e. <35°) thrust fault structures

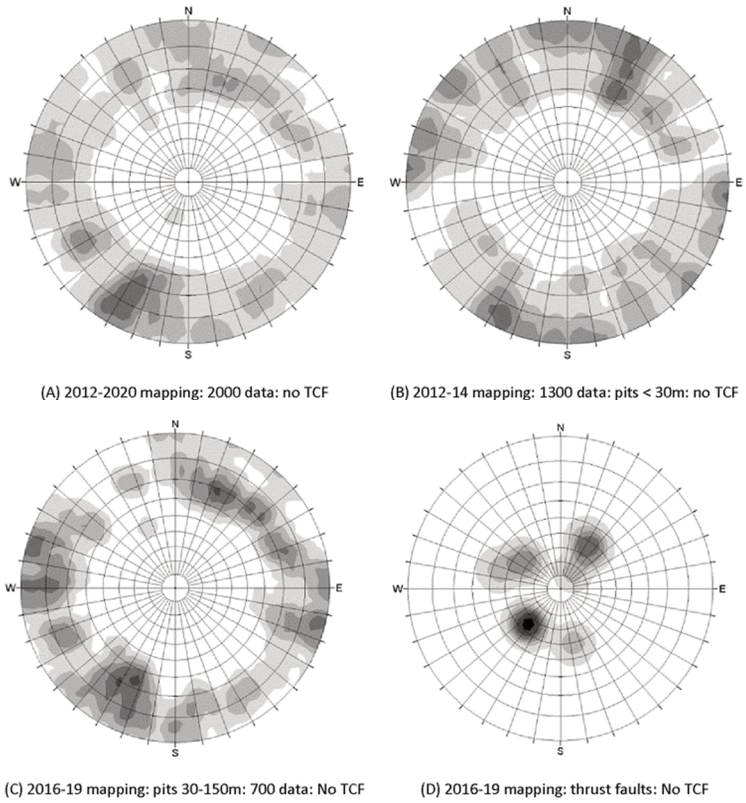

Figure 10 Mapping: stereographic projection plots (Terzaghi correction factor (TCF) for sampling bias)

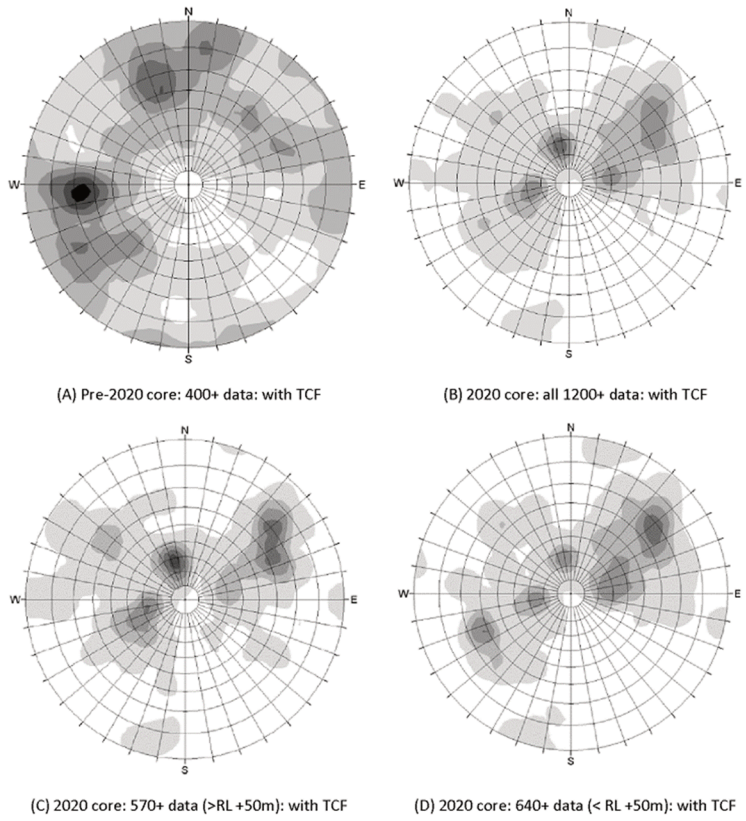

Figure 11 Core: stereographic projection plots

Figure 12 shows models for structure length, infill type and thickness, and Barton's surface roughness. The median length is 10 m; with only 10% being longer than 50 m. Weak infill (i.e. clay, chlorite, talc,

manganese, breccia and/or blends of these) exists along 90% of structures. The median infill thickness is 0.4 mm and <2 mm of infill occurs on 70% of structures. Barton's small-scale joint surface roughness is six with a standard deviation of 1.5. Large-scale undulation/waviness (i.e. stated in degrees) along structures is about 4–5° with a standard deviation of 4°.

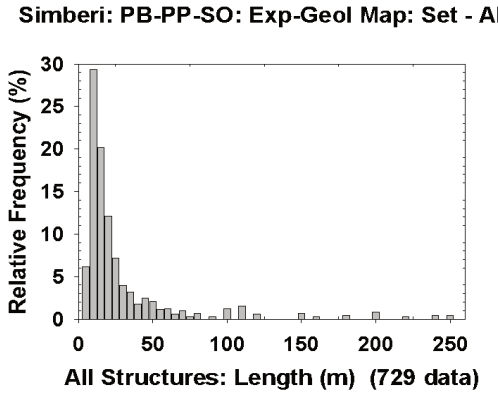

(A) 2016-19 mapping: structure length relative frequency

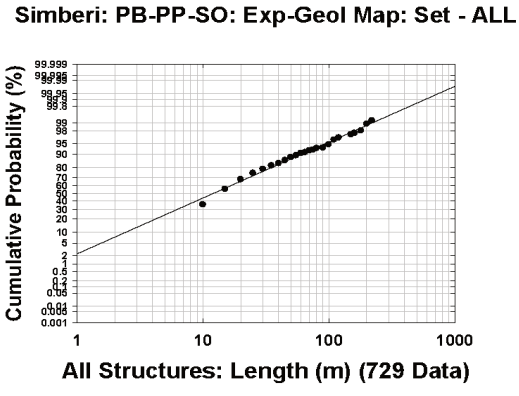

(B) 2016-19 mapping: structure length cumulative frequency

General Model (based on 1433 data)	
Clean (No Infill)	2%
Weak Infill (Clay, Chlorite, Talc, Manganese)	79%
Weak Breccia with Clay / Chlorite	11%
Strong (iron oxides) with minor Clay / Chlorite	4%
Strong (iron oxides, pyrite, quartz); no Clay	4%

(C) 2020 cores: Infill type

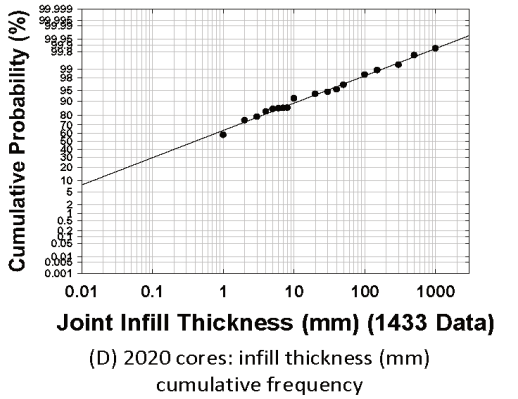

(D) 2020 cores: infill thickness (mm) cumulative frequency

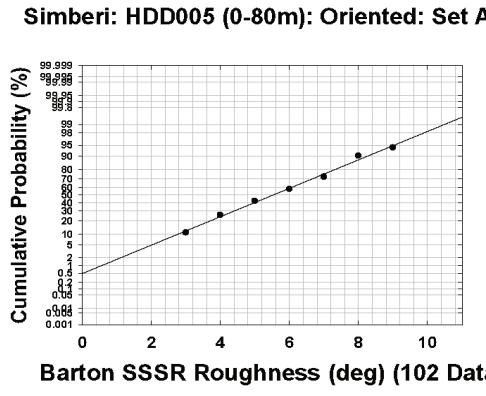

(E) 2020 cores: small-scale Barton roughness (1-10 scale): cumulative frequency

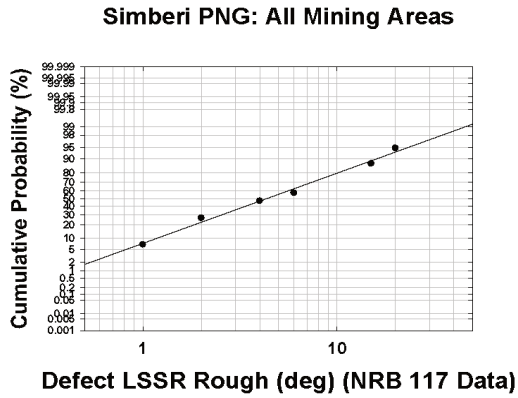

(F) 2020 mapping: large-scale surface undulations (degrees): cumulative frequency

Figure 12 Slope mapping and core data: statistical models for structure length, infill and roughness

5 Intact rock properties

5.1 Unconfined compressive strength

Core logging estimation of UCS strength proved a major challenge due to the Simberi volcanic rocks often containing significant size breccia particles (5–80 mm diameter, see Figure 8) or being closely fractured, flow-layered or veined. Despite best efforts, it was difficult to find adequate-length core samples devoid of

breccia fragments or structural flaws. In this selection bias of the least-flawed cores, laboratory results represent an upper-bound UCS strength model. Even then, the majority of laboratory UCS samples still failed partially along breccia particle-matrix boundary or some structural feature.

Reconciling core logging-estimated UCS with laboratory tested UCS strength showed that whilst a near 1:1 correlation (with correlation coefficient >0.9) was sometimes achieved, cross-plot scatter was often wide (i.e. with correlation coefficient for trend lines of 0.5–0.6). Of greater concern was that core logging tended to overestimate UCS by 50–350%, with the average over-estimation being 200%. The poor estimation was addressed by doubling the number of laboratory tests and by basing slope design UCS on laboratory results rather than core logging estimates. Figure 13a shows best, and Figure 13b shows worst, correlations between core-estimated and laboratory-derived UCS.

Representative UCS samples were selected over the full RL depth range being investigated. Figure 14a shows the scatter of individual laboratory UCS results with decreasing RL depth. Figure 14c shows cumulative frequency distribution on a logarithmic probability scale.

Median UCS is 4–5 MPa; one standard deviation range is 0.7–25 MPa; 70% of samples were <10 MPa; and UCS >50 MPa was rare. Figures 14b and 14d show the trend for UCS averaged in 25 m RL depth intervals. Figure 14b mean trend line between RL 25–125 m is influenced by few outlier UCS results >50 MPa. The regression equation in Figure 14d was adopted for the design of pit slopes below RL 150 m. The UCS above RL 150 m is typically <2 MPa; often as low as 0.5–1 MPa.

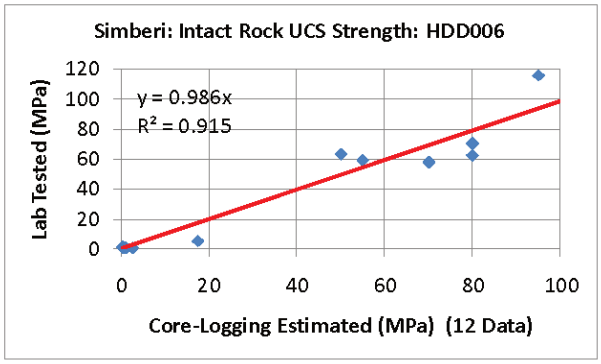

(A) Hole HDD006: best UCS estimate

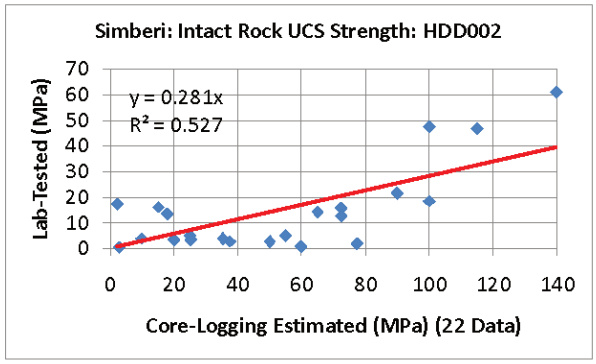

(B) Hole HDD005: worst UCS estimate

Figure 13 Core logging unconfined compressive strength (UCS) estimate versus laboratory test: (a) Best; (b) Worst

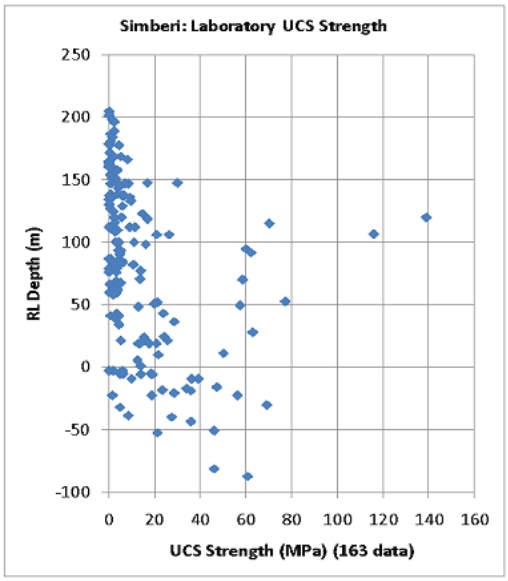

(A) Individual laboratory UCS and RL (m)

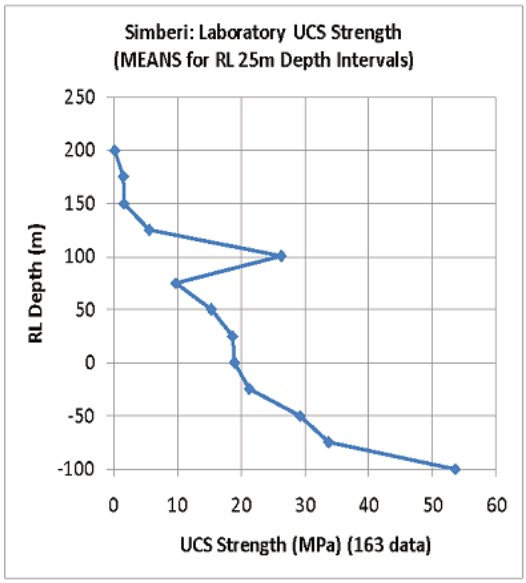

(B) Mean laboratory UCS over 25m RL depth

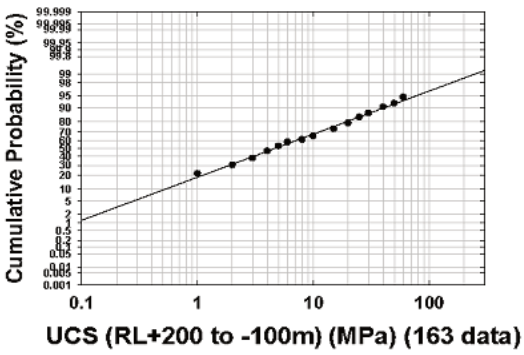

(C) Laboratory UCS cumulative frequency distribution on probability scale

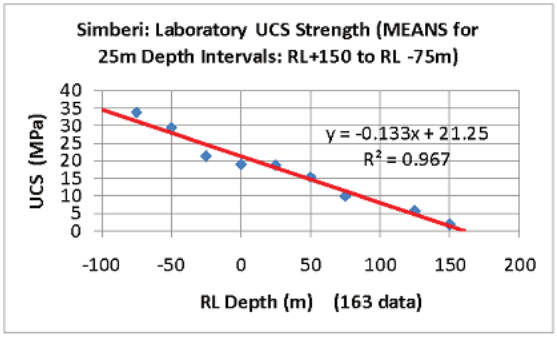

(D) Trend-line for laboratory UCS averaged over 25m RL depth (i.e., RL+150m to RL -75m)

Figure 14 Laboratory-test unconfined compressive strength (UCS): (a) Individual results; (b) Data averaged over 25 m relative length (RL) depth intervals; (c) Cumulative frequency on logarithmic probability scale; (d) Trend with RL (m) depth

5.2 Tensile strength and compressive-tensile strength relationship

Brazilian tensile and Is(50) point-load tests were completed for 50% of UCS-tested samples. Tensile strength was also calculated from rock triaxial tests (RTX) and consolidated undrained triaxial soil tests (CU).

Figures 15a to 15d cross-plot UCS with tensile strength. UCS to Is(50) ratio is 11–13; UCS to Brazilian is 9–10 and UCS to TRX/CU derived tensile strength is 5–6. Correlation coefficient for Is(50) data is low (i.e. 0.4); better coefficients (i.e. 0.7–0.8) exist for Brazilian and RTX/CU data. In view of variable particle sizes in volcanic breccia rocks, poorly defined UCS to Is(50) correlation trend lines are not surprising.

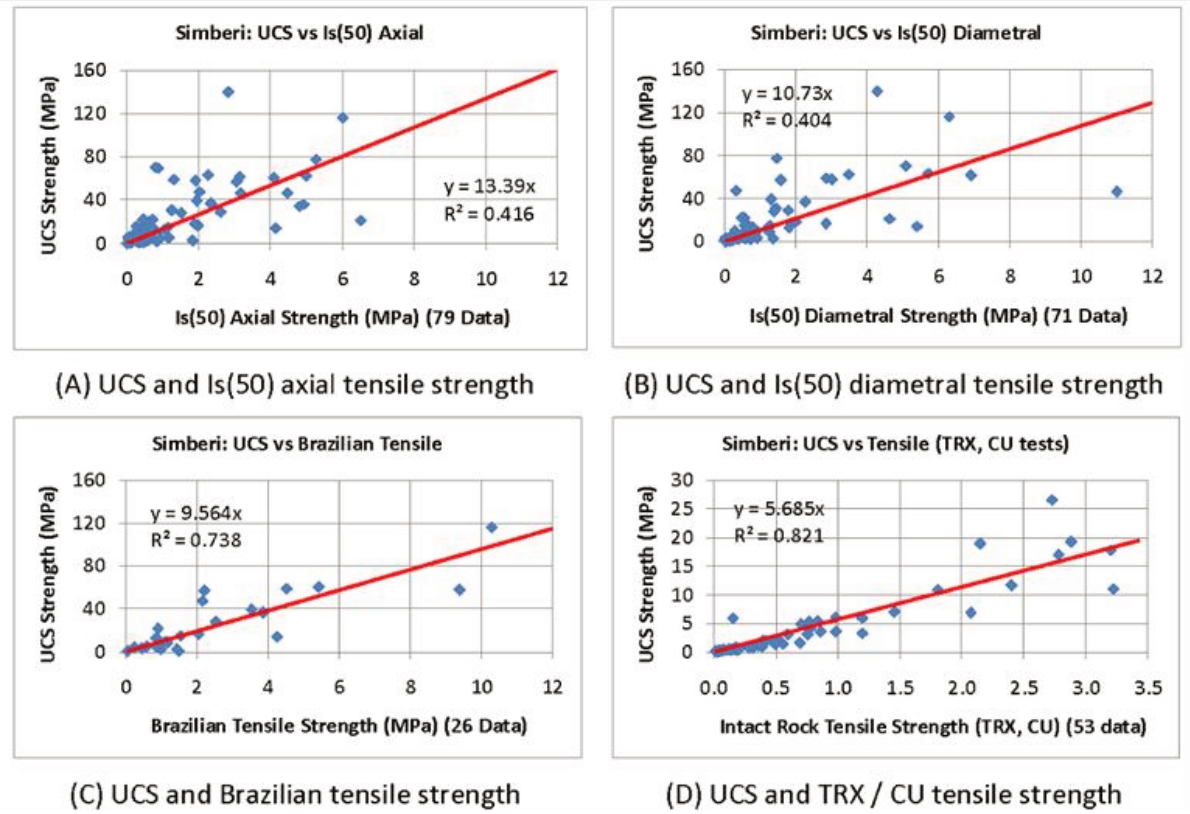

Figure 15 Unconfined compressive strength (UCS) versus tensile strength: (a) Is(50) axial; (b) Is(50) diametral; (c) Brazilian; (d) Tensile from rock triaxial (RTX) and consolidated undrained (CU) soil triaxial tests

5.3 Triaxial and direct shear strength

Triaxial and direct shear laboratory tests were carried out on very low intact rock strength cores. Such weak rocks represent most ground above RL 150 m, and often comprise significant zones below that level. For most open pits, occurrence of weak rock and brecciated zones decreased with decreasing RL depth. Whilst some direct shear tests were purposely planned at the outset, most were done when samples initially earmarked for triaxial tests were disturbed along some part of their length (i.e. insufficient undisturbed sample length for triaxial test but enough length for direct shear tests).

Figures 16a and 16b show cross-plots of effective friction angles versus cohesion. Whilst a linear trend exists for the triaxial results, it has a low correlation coefficient of 0.35.

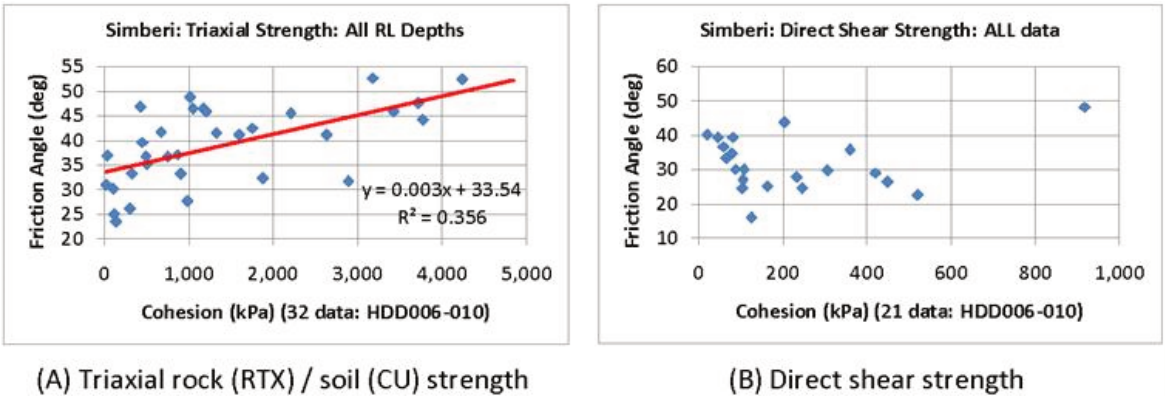

Figure 16 (a) Triaxial; (b) Direct shear peak strength results

In general, triaxial strength increased with decreasing sample RL depth, with the highest laboratory strengths observed from samples in the RL +50 m to -50 m depth range. The interpreted triaxial strength model for highly weathered volcanic breccia intact rock has an effective peak friction angle of 39° with a standard deviation of 8° and cohesion of 1.35 MPa with a standard deviation of 1.25 MPa.

There is no obvious trend in the direct shear results. The interpreted direct shear strength model for brecciated zones has an effective peak friction angle of 31°, with a standard deviation of 7°, and cohesion of 0.20 MPa with a standard deviation of 0.15 MPa.

5.4 Density

As per Figure 17, rock density increases and moisture content (%) decreases with decreasing RL depth. The mean dry density ranges from 17 kN/m^3 at RL +200 m to 25 kN/m^3 at RL -100 m. Corresponding mean moisture contents and wet densities are 19 and 3%, and 19.5 and 25.5 kN/m^3, respectively.

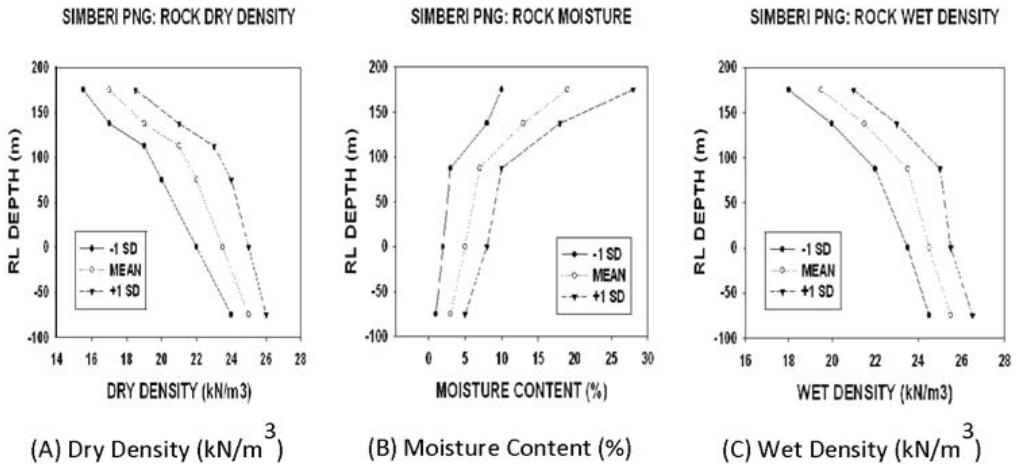

Figure 17 (a) Dry density, (b) Moisture content; (c) Wet density (SD is standard deviation)

6 Rock mass characterisation and Hoek–Brown strength

6.1 Simplified rock quality designation trend with relative length depth

To mitigate the wide scatter of data, RQD core logging data was averaged over 25 m RL depth intervals; Figure 18 shows the resulting mean trend.

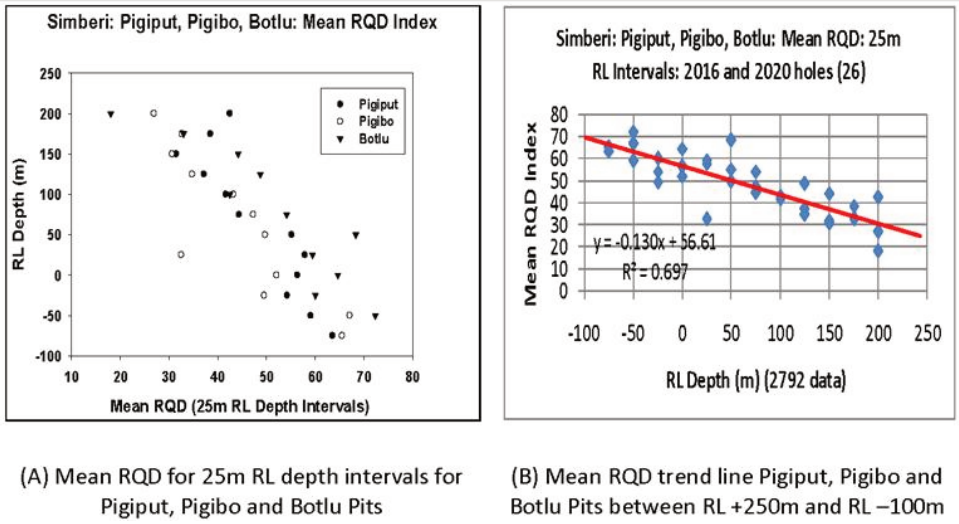

Figure 18 Simberi: simplified rock quality designation (RQD) model for variability with relative length (RL) depth

In Figure 5, the RQD scatter was assessed statistically to provide input to slope design. There are two scatter/standard deviation concepts.

The first concept reflects the RQD scatter within each specific 25 m RL depth interval of the seven geotechnical holes drilled in 2020. These holes were logged in 2 m downhole depth intervals. Within each 25 m RL depth interval, 13–15 RQD data exist in each hole; a cumulative total of 90–100 RQD data for the seven holes combined. Figure 19a shows the mean and ±1 standard deviation bounds for this data.

The second concept reflects scatter between RQD mean values computed for each geotechnical hole at the designated RL depth interval. With seven holes, Figure 19b reflects the statistical spread of seven mean values. Mean trends in Figures 19a and 19b are the same, but standard deviation bounds are much reduced for grouped data. This reduction is consistent with sampling theory logic, as per Figures 19c and 19d.

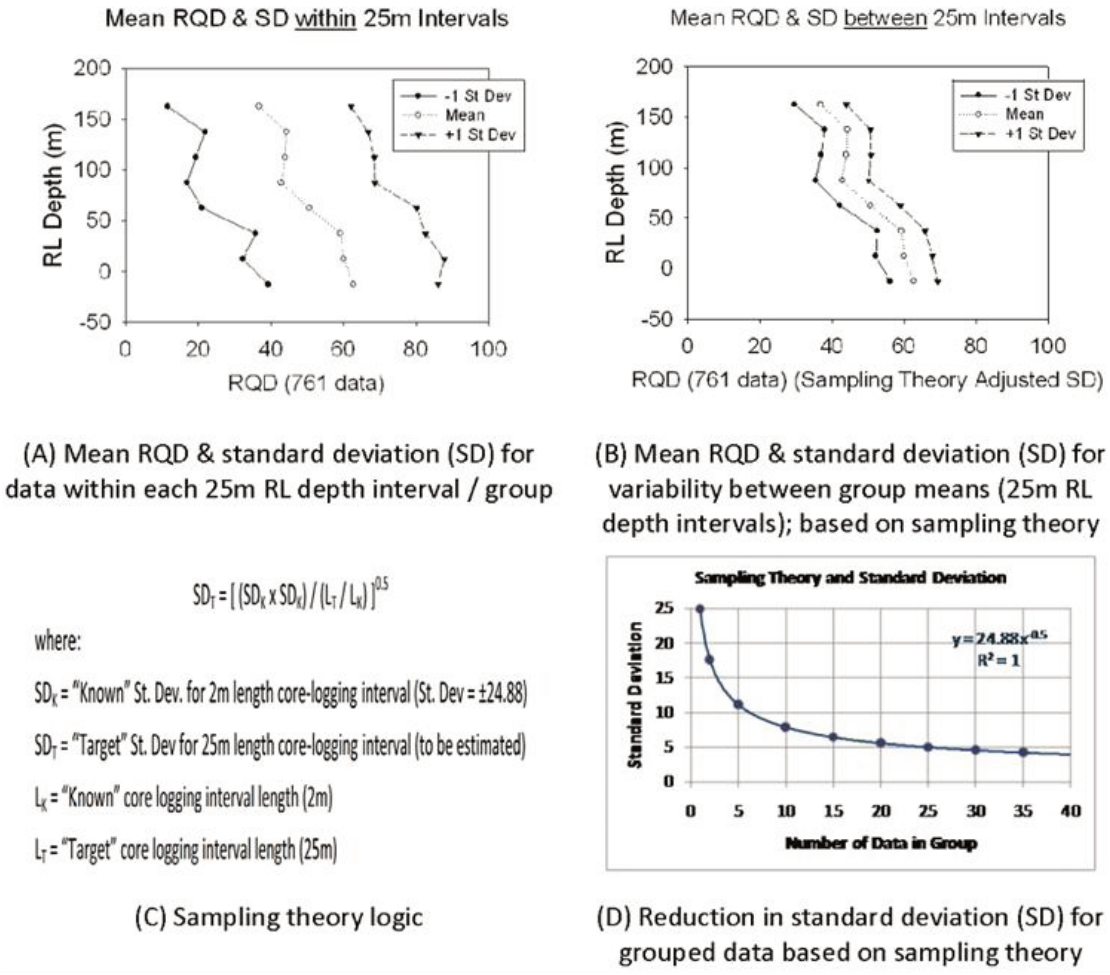

(A) Mean RQD & standard deviation (SD) for data within each 25m RL depth interval / group

(B) Mean RQD & standard deviation (SD) for variability between group means (25m RL depth intervals); based on sampling theory

(C) Sampling theory logic

(D) Reduction in standard deviation (SD) for grouped data based on sampling theory

Figure 19 Simberi: simplified rock quality designation (RQD) model for variability with relative length (RL) depth

6.2 Hoek–Brown geological strength index

Geological strength index (GSI) was derived on the basis of RQD rating and joint condition method detailed in Hoek et al. (2013), per Equation 1:

$$GSI = (1.5 \times (\text{joint caondition})) + (0.5 \times RQD) \quad (1)$$

Attributes considered in joint condition are structure length, aperture (infill thickness), surface roughness, infill type and structure wall rock weathering. Statistical models for these are detailed in this paper.

Per Baczynski (2016c) for slope applications, Rosenblueth (1975, 1981) method of statistical moments was used to assess the statistical spread of GSI values.

6.3 Trend in Hoek–Brown rock mass strength

RQD and UCS models improve linearly with decreasing RL depth. Accordingly, a layered rock mass strength model was adopted. Per Figure 20, each material layer was 25 m thick. The stability impact of specific known faults was individually considered. Other inputs to Hoek–Brown strength are m_i and D. The published values for volcanic breccia m_i of 19 with standard deviation of 5 was adopted. The same mean m_i was interpreted from the laboratory triaxial strength results; but the achieved correlation coefficient was very poor. Parameter D considers blasting disturbance, with 0.7 adopted for disturbed slopes.

For high m_i and low UCS, Hoek–Brown strength curve almost passes through the origin of normal-shear stress plots, with near-zero cohesion at low normal stress. Such near-zero cohesion is at variance with stability back-analyses of existing slopes. Based on back analyses, Hoek–Brown strength curve was adjusted upwards by 0.1 and 0.05 MPa for blasting-undisturbed (D = 0) and blasting-disturbed (D = 0.7) conditions, respectively.

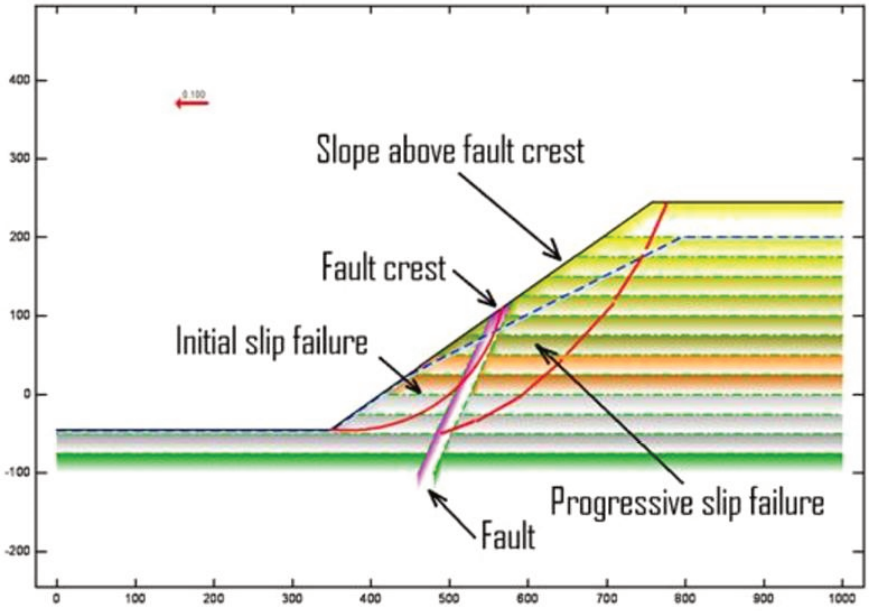

Figure 20 Layered geotechnical strength model and position of known individual fault

Development of a common, horizontally layered, strength model has stability analysis advantages. After the strength model is entered into the software, pit slope profiles (i.e. designated in terms of pit crest and floor RL depths) are easily defined and stability assessed within such a layered rock mass strength sequence.

Per Figure 20, the stability impact of known major faults in specific slopes was individually considered.

6.4 Earthquake risks

Preliminary earthquake risks (on Richter scale) were assessed in 2016–2018 investigations; slope stability analyses considered a parametric range of conditions. Swaisgood (2020) quantified the risks for Simberi Island, per Figure 21. Slope design lives of 25, 50 and 100 years are considered. The maximum 84th percentile peak ground acceleration (PGA) from maximum credible earthquake data is 0.23 g, hence the PGA x-axis in Figure 21 is truncated at this magnitude.

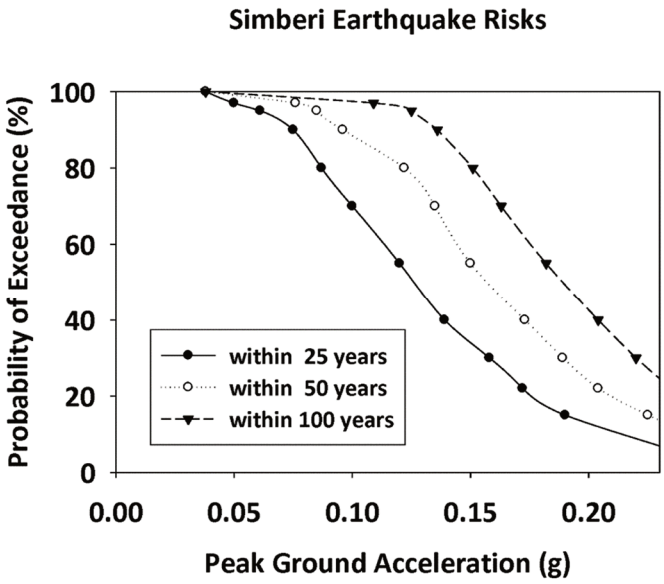

Figure 21 Earthquake risks: probability of exceedance for 84th percentile peak ground acceleration (Swaisgood 2020)

6.5 Groundwater

Rainfall is 3–5 m/year. Groundwater levels rise during the wet season as attested by an increase in artesian bore flow rates. The pre-mining watertable is interpreted to coincide with the oxide-sulphide ore boundary. This boundary significantly mirrors pre-mining surface topography. Fully saturated slopes have low stability and some groundwater drawdown is necessary to achieve acceptable Factors of Safety in slope design. Figure 20 (in Section 6.3) shows the required partial drawdown (dashed blue line). This drawdown profile assumes that slopes below sea level will be saturated.

7 Conclusion

Simberi pit slopes comprise volcanic breccias, porphyry intrusives and minor sedimentary strata.

Geotechnical investigation methodology, challenges, results, data trends, laboratory-derived parameters and pit slope rock mass strength models are presented and discussed.

Structural geology is complex and variable but major faults likely to significantly impact slope stability are reasonably well defined. Orientated cores confirm that the same structural patterns persist with depth.

Core logging estimation of UCS strength proved a major challenge, with strength often being over-estimated. Due to the latter, laboratory testing was doubled and final slope design is based on laboratory data rather than core logging estimates.

To counter wide data scatter and develop meaningful trends, geotechnical data was partitioned into 25 m RL depth intervals. This approach yielded convincing linear trends for RQD, and laboratory-derived UCS strength and rock density. The developed geotechnical models are valid for Pigiput, Pigibo and Botlu pits.

Initial aim was to consider both the Hoek–Brown and Step-Path rock mass strength models. However, Step-Path models may be confounded when UCS of intact rock is <10 MPa. This situation arises because Barton's joint strength often exceeds Hoek–Brown rock mass strength for UCS <10 MPa. Since the mean intact rock UCS is <10 MPa in the Simberi rock mass above RL 75 m, a Step-Path strength model could only have been developed for the lower third of Pigiput Pit slope but not for the Botlu and Pigibo pits where UCS <10 MPa persists to the respective pit floors. With limited opportunity to use Step-Path strength, overall pit slope design is based on the Hoek–Brown method.

A Simberi-specific earthquake risk model was developed for slopes with a 25, 50 and 100-year design life.

Future geotechnical core data should also be similarly processed in 25 m RL depth intervals to check if the presently observed trends persist and are valid for other Simberi pits.

Acknowledgement

Norbert Baczynski thanks Simberi Gold Company Limited and St Barbara Pty Ltd for the opportunity to have been able to work on the Simberi project since 2016 and to co-author this paper.

References

Baczynski, NR 2016a, *Pre-Feasibility Study: Pit Slope and Waste Dump Design Geotechnical Review*, Prime Geotechnics Pty Ltd, internal report 2016-001, produced for Simberi Gold Company Limited.

Baczynski, NR 2016b, *Geotechnical Stability Analysis of Existing Pit Slopes, Access Ramps and Waste Rock Dumps*, Prime Geotechnics Pty Ltd, internal report 2016-003, produced for Simberi Gold Company Limited.

Baczynski, NRP 2016c, 'Simplified Step-Path method for rock slopes', in PM Dight (ed.), *APSSIM 2016: Proceedings of the First Asia Pacific Slope Stability in Mining Conference*, Australian Centre for Geomechanics, Perth, pp. 255–270, https://doi.org/10.36487/ACG_rep/1604_13_Baczynski

Baczynski, NR 2017, *Simberi Gold Mine, Papua New Guinea: Pit Slopes and Waste Dumps Annual Geotechnical Review – 2017*, Prime Geotechnics Pty Ltd, internal report 2017-003, produced for Simberi Gold Company Limited.

Baczynski, NR 2018, *Simberi Gold Mine, Papua New Guinea: Pit Slopes and Waste Dumps Annual Geotechnical Review – 2018,* Prime Geotechnics Pty Ltd, internal report 2018-002, produced for Simberi Gold Company Limited.

Baczynski, NR 2019, 'GSI adjustments for directional Hoek-Brown Strength calibrated by Step-Path case studies', *Australian Geomechanics Journal*, vol. 54, no. 3, pp. 51–78.

Baczynski, NR 2020, *Simberi Gold Mine, Papua New Guinea: Sulphide Slopes Study Geotechnical Review: Final Report (Rev2)*, Prime Geotechnics Pty Ltd, internal report 2020-002, produced for Simberi Gold Company Limited.

Barton NR & Choubey, V 1977, 'The shear strength of rock joints in theory and practice', *Rock Mechanics*, vol. 10, no. 1–2, pp. 1–54.

Dames & Moore 1989, Geotechnical report for Kennecott Niugini Mining Joint Venture, Barry McMahon.

Douglas Partners 2005, *Geotechnical Testing of Rock Core, Simberi Island, Sorowar Pit*, internal report ref. no. PSS: MPG: MAA Project 40102, produced for Allied Gold Limited.

Golder Associates Pty Ltd 1996, *Geotechnical Aspects, Mining Feasibility, Simberi Gold Project, Tabar Islands, Papua New Guinea*, internal Report Ref No 96640096(B), produced for Lycopodium Pty Ltd and for Nord Resources (Pacific) Pty Ltd.

Golder Associates Pty Ltd 2003, *Geotechnical investigation: Simberi Gold Mine: proposed development of Botlu South and Pigibo Resources, Simberi Island, New Ireland Province, Papua New Guinea*, internal report ref. no. 03639011(C), produced for Allied Gold Limited.

Golder Associates Pty Ltd 2010, *Mining section for Simberi Island Sulphide PFS*, internal report ref. no. 107641039-001-R-Rev0, produced for Allied Gold Limited.

Golder Associates Pty Ltd 2011, *Interim Geotechnical Report for Pigiput and Pigibo*, internal technical memorandum ref. no. 107641039 007 TM Rev0, produced for Allied Gold Limited.

Hoek, E, Carter TG & Diederichs MS, 2013, 'Quantification of the Geological Strength Index chart', *Proceedings of the 47th US Rock Mechanics/Geomechanics. Symposium,* American Rock Mechanics Association, Alexandria.

Jones, S 2013, *Structural models for the Simberi Gold Deposits, PNG*, internal report, produced for St Barbara Limited.

Jones, S 2014, *Updated Structural Model for the Gold Deposits on Simberi Island, PNG*, internal report, produced for St Barbara Limited.

McMahon Associates 1986, Geotechnical report for for Kennecott Niugini Mining Joint Venture, Barry McMahon.

Norman, A 2012, *Pigibo, Pigiput & Monum Creek Structural Interpretation*, internal memorandum, GeoCentric Explorations Pty Ltd.

Rosenblueth, E 1975, 'Point estimates of probability moments', *Proceedings of the National Academy of Sciences*, vol. 72, no. 10, pp. 3812–3814.

Rosenblueth, E 1981, 'Two-point estimates in probabilities', *Applied Mathematical Modelling*, vol. 5, no. 2, pp. 329–335.

Swaisgood JR 2020, Development of seismic parameters and ground motion records for seismic analysis of the Simberi Mine waste dumps and pit slopes', internal report, produced for Simberi Gold Company Ltd.

Terzaghi, RD 1965, 'Sources of error in joint surveys', *Géotechnique*, vol. 15, no. 3, pp. 287–304.